Slenderness Effect for The Composite RC Columns with Steel Angles at The Corners; Experimentally and Analytically

[a] Ahmed Abdellatif, [b] Nehal M. ayash, [c] Ahmed H. Ali and [d] Hala Mamdouh

[b, c, d] Associate Professor, Civil Engineering Department, Faculty of Engineering at Mataria, Helwan University,11718, Cairo, Egypt.
[a] M. Sc. Student, Civil Engineering Department, Faculty of Engineering at Mataria, Helwan University,11718, Cairo, Egypt.

[b] nehal82ayash@m-eng.helwan.edu.eg,[a] Ahmedabdelatef2012@m-eng.helwan.edu.eg
[c] Ahmed.Ali@usherbrooke.ca, [d] Hala_mamdouh@m-eng.helwan.edu.eg

Abstract

The study focuses on the application of composite columns, utilizing four steel angles at the corners of the concrete column welded together with a transverse plate, and contrasting the experimental findings with those produced by structural analysis programs using ANSYS. Three square composite columns are included in the experimental test program under axial compression, and the primary variables are the longitudinal reinforcement ratio and steel angle thickness. Investigations are conducted into the axial and horizontal deformations, load capacity, failure mode, and axial and lateral strains of composite columns. In order to review the impact of the slenderness ratio on the behavior of composite columns for parametric study, more numerical models are utilized. The results indicate that there are two primary phases to the failure process. Localized buckling in the longitudinal reinforcement occurs in the second stage, after the concrete cover has been crushed or spalled in the first stage. The impact of steel angle thickness according to experimental results: axial strain, lateral strain, horizontal displacement, and axial displacement decrease with increasing steel angle thickness. The percentage of decrease for axial displacement is between 11% and 20%; for horizontal displacement, it is between 16% and 20%; for axial strain, it is between 4% and 10%; and for lateral strain, it is between 13% and 22%. But the load capacity increases with increasing steel angle thickness, the percentage of increase for load capacity is between 16% and 23%. The convergence rate between the analytical model and the experimental results ranged from 2% to 6% for load capacity, and 5% to 14% for axial displacement. This indicates that an analytical model that was created with the aid of the ANSYS software was able to accurately anticipate the failure load, axial deformation, and failure modes. From the

parametric results obtained analytically, it can reach that with the same reinforced angle thickness, a higher slenderness ratio resulted in greater axial distortion with no impact on load capacity. This warning is particularly noticeable for columns that have smaller reinforced angles as opposed to thicker ones. If there is no obvious buckling, the influence of the column height reduces as the column height and the steel angle thickness grow. In contrast to short columns, slender columns' load capacity can be increased by increasing the thickness of the reinforcing steel angle, which also results in a greater reduction in axial distortion. Energy absorption rises with increasing slenderness ratio for thinner reinforced angles but falls with increasing slenderness ratio for broader reinforced angles.

Keywords: composite columns; steel angles; load capacity; slenderness ratio; axial displacement; axial compression

1. Introduction

Several experimental and analytical studies were conducted to ensure the structural efficiency of composite columns as their employment in long-span constructions, skyscrapers, and industrial buildings has grown in recent years (Kim et al. 2011). Concrete-encased steel (CES) and concrete-filled steel tube (CFT) are the two basic types of concrete composite columns. The rebar that is used and the locations in which it can be positioned, such as in I-beam sections or steel angles, determine the various types of encased composite columns (Lacki et al. 2017, Kumar and Sai 2019). The main benefit of utilizing steel angles for composite columns instead of I-beam sections in encased columns is that the former have more confined concrete than the latter (Zhang et al. 2019). Based on the transverse steel plates, there are two varieties of composite columns having steel angles (Kim et al. 2021, Kim et al. 2020). There are two types of steel angles: the first type involves welding the plates to them, while the second type involves bolting the plates to them (Badalamenti et al. 2010, Eom et al. 2021). Aiming to investigate additional parameters influencing composite columns, prior research and studies were explored to learn about the outcomes. In a study by Kim et al. (2013), a total of six square column specimens with varying heights and cross-sections under eccentric axial compression were tested. Two of the specimens were concrete-filled steel tube columns, and the remaining four were concrete-encased steel columns made of high-strength steel and concrete. The behavior of the two types of columns was compared. Despite the presence of local buckling, they observed that the concrete-filled tube columns demonstrated a good indication of structural performance. Eom et al. (2013) compared between the prefabricated steel-reinforced concrete specimens and the conventional composite specimen (H-section) using a total of eight square column specimens with a height of 4500 mm and cross-section measurements of 400 mm by 400 mm for three specimens and 500 mm by 500 mm for five specimens. The prefabricated steel-reinforced concrete specimens demonstrated greater flexural strength and stiffness than the conventional composite specimen (H-section), and AISC 360-10 (2010) states that the bearing strength of the welded transverse bars was used to estimate the bond strength between concrete and steel angles. In 2018, Vummaneni and Reddy

examined the strength, deflection, and surface strains of composite reinforced concrete columns, and compared them with traditional columns through testing a total of four short square column specimens, each measuring 150 x 150 mm in cross-section and 1000 mm in height. Two specimens were strengthened with four ϕ12 mm specimens, while the other two specimens were reinforced with four equal steel angles measuring (25 x 25 x 3) mm. When employing steel angles, they observed that the percentage of increased strength reached 20% and the deflection decreased to 2.38 times. In a study by Hwang (2018), Five square column specimens with a cross section of 500x500 mm and steel ratio of 2% with different steel cross section (steel angle and IPE) were tested, allowing for the comparison of a prefabricated steel-reinforced concrete (PSRC) composite column using steel angles and a conventional concrete-encased steel (CES) composite column. They observed that the axial load capacity, deformation capacity, and corner angles of the PSRC column are more precise than those of the CES columns, and that the PSRC column's flexural strength and stiffness can rise by up to 30% in comparison. The effects of confinement effect, local buckling, and premature cover-spalling were numerically discussed by Kim and Hwang (2018) for the results of previous experimental studies by testing a total of sixteen square column specimens under concentric and eccentric axial compression, with varying cross-sections (260 mm × 260 mm, 400 mm × 400 mm, and 500 mm × 500 mm) and heights of 1500 mm. They observed that the early spalling of concrete cover and the effect of local buckling of steel angles on confinement, which are the special local failure mechanisms of columns. Ibrahim et al. (2018) investigated the effects of lateral tie spacing and longitudinal reinforcement type on the behavior of high-strength concrete (HSC) specimens under axial compression. A total of 12 square specimens with a cross-section of 210 × 210 mm and a height of 600 mm were tested under concentric axial compression. Each group of specimens has a different stirrup spacing (50mm, 100mm, 200mm, and 400mm). They observed that all specimens reinforced with steel angle sections exhibited greater ductility and axial load than specimens reinforced with steel bars. At the same stirrups spacing, the percentage of the load decrease reached 15.1% when the specimens reinforced with steel angle sections had their stirrups spaced from 50 mm to 400 mm. Rong and Shi (2020) studied the mechanical properties of angle steel frame confined concrete columns (ASFCs). Furthermore, to investigate the effect of confinement on concrete under axial load, a total of twelve square column specimens with a concrete cross-section measuring 300 mm by 300 mm and varying column heights under concentric axial load were evaluated. They observed that the steel angles caused confinement to form on the concrete. Concrete's mechanical properties increased as a result of this. For the same confining stress, low-strength concrete has stronger confining than high-strength concrete. When the size of the steel angle bars is increased, the strength of the concrete is further improved. Higher concrete confinement occurs when the steel batten spacing is narrower. Before the maximum load of the angle steel frame confined concrete columns, all strains reach the yield state.

2. Research Significant

The study focuses on the use of composite columns, which are made of concrete columns with four steel angles at the corners that are welded together with a transverse plate. It compares the results of the experiments with those generated using ANSYS structural analysis software. More numerical models are used to examine how the slenderness ratio affects the behavior of composite columns for parametric study.

3. Experimental work

3.1. Specimen Details

Three columns with a concrete cross section of 200 x 200 mm and a column height of 1200 mm make up the experimental test program. A1(L50-T3-S200), A2(L50-T4-S200) and A3(L50-T5-S200) are the first, second and last specimens, reinforced with four equal steel angles with dimensions 50 x 3 mm, 50 x 4 mm and 50 x 5 mm and having a steel ratio of 2.91%, 3.8%; and 4.75%. The transverse reinforcement is in the form of a 40x4 mm plate spaced 200 mm apart as demonstrated in **Table 1 and Figure 1**. The leg of steel angle is indicated by the symbol (L), the thickness of steel angle is indicated by the symbol (T), and the spacing between transverse reinforcement is indicated by the symbol (S).

Table 1. The details of all tested samples

Columns		A1 (L50-T3-S200)	A2 (L50-T4-S200)	A3 (L50-T5-S200)
Cross section dimensions (mm)		200×200	200×200	200×200
Height (mm)		1200	1200	1200
Longitudinal reinforcement	Type	4 equal steel angles	4 equal steel angles	4 equal steel angles
	Dimensions (mm)	L 50×3	L 50×4	L 50×5
	Ratio %	2.91	3.8	4.75
Transverse reinforcement	Type	plate	plate	plate
	Dimensions (mm)	40×4	40×4	40×4
	Spacing (mm)	200	200	200

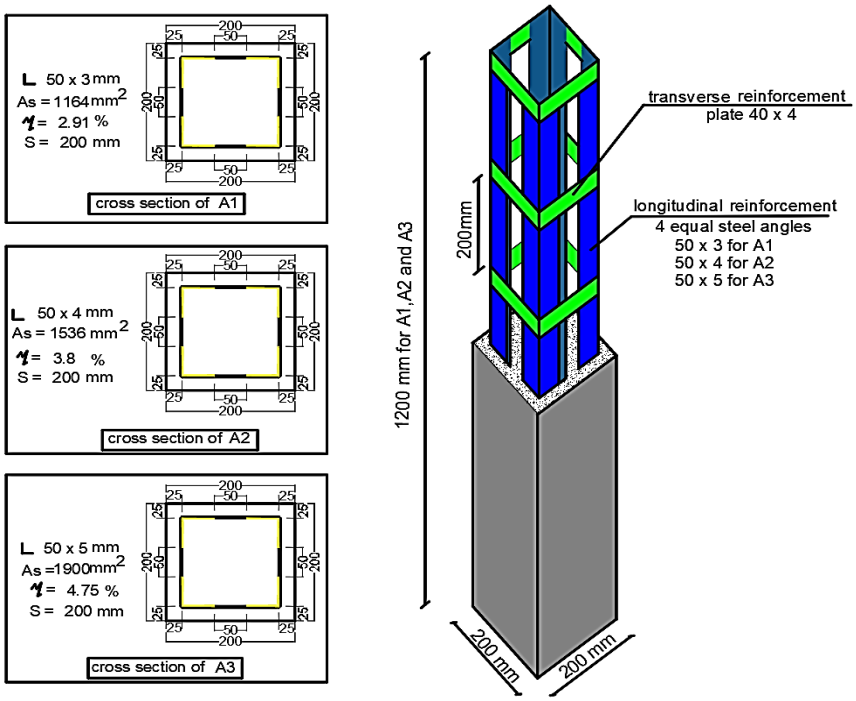

Figure 1. Cross section geometry and details for specimens A1, A2 and A3

3.2. Material Properties

3.2.1. Concrete

Cement, water, fine aggregate and coarse aggregate make up the concrete mix. The maximum aggregate size for the concrete mix was 20 mm, the water cement ratio was 0.55, and the cement content was 382 kg/m^3. Crushed aggregate was utilized as the coarse aggregate. To ascertain the workability, a slump test was performed; the result was 35mm. The amounts of each component of the concrete mix required to generate 1 m3 are listed in **Table 2**. To determine the compressive strength (f_{cu}), a total of 15 cubic samples with standard cube dimensions of 150 x 150 x 150 mm were manufactured. To determine the modulus of rupture (f_{ctr}), a total of five cylindrical samples with standard cylinder dimensions of 150 x 300 mm were constructed. Every sample was cured by immersing it in clean drinking water. The mechanical properties after 28 days are listed in **Table 3**. The failure shape of standard cylinders and cubes is displayed in **Figure 2**.

Table 2. Concrete mix proportion

Material	Coarse Aggregate (Kg/m^3)	Fine Aggregate (Kg/m^3)	Cement (Kg/m^3)	Water (Liter/m^3)
Concrete	**1196**	**563**	**382**	**210**

Table 3. Concrete mechanical properties after 28 days

Compressive strength f_{cu} (MPa)	Modulus of rupture f_{ctr} (MPa)	f_{ctr} / f_{cu}	Modulus of elasticity E_c (MPa)
37.3	28.4	0.76	30300

(a) Standard Cubes **(b) Standard cylinder**

Figure 2. Failure shape of (a) Standard cubes (b) Standard cylinder

3.2.2. Reinforcing Steel

By averaging the results of three samples for each type of steel reinforcement, a tensile test was conducted to determine the yield tensile strength, ultimate tensile strength, and modulus of elasticity for steel reinforcement. Steel reinforcement's mechanical properties are listed in **Table 4**. The failure shape of the steel reinforcement is displayed in **Figure 3**.

Table 4. Mechanical properties of steel reinforcement

Shape	Leg Width (mm)	Thickness (mm)	Area (mm^2)	Yield Tensile Strength (MPa)	Ultimate Tensile Strength (MPa)	Modulus of Elasticity (MPa)
Angles	50	3	291	364.6	483.3	20880
	50	4	384	351.7	428.3	22240
	50	5	475	326.4	417.6	21832
Plate	40	4	160	342.5	485	21081

(a) Samples of angle Thickness 3mm **(b) Samples of angle Thickness 4mm**

(c) Samples of angle Thickness 5mm **(d) Samples of plate Thickness 4mm**

Figure 3. Failure shape of steel reinforcement (Angles and Plate)

3.3. Test Set-up

For each column in the test setup, there are three LVDTs and two steel strain gauges:(a) To measure the horizontal displacement, the first LVDT was positioned in the middle of the span. (b) To measure the horizontal displacement in the opposite direction, the second LVDT is fixed near the center of the span in the other direction of the first LVDT. (c) The third LVDT, which is fixed at the top of the column, measures the vertical displacement as shown in **Figure 4**. Additionally, two steel strain gauges were positioned, one in the center of the longitudinal reinforcement and the other in the middle of the transverse reinforcement as shown in **Figure 5**.

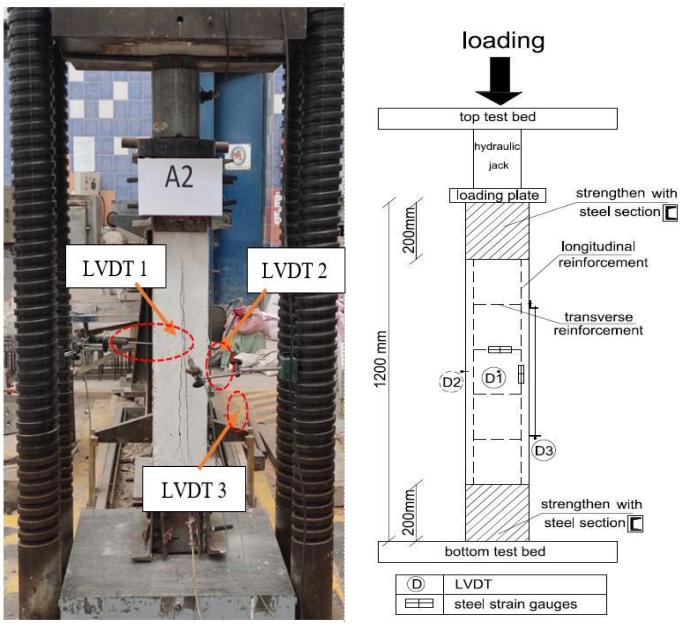

Figure 4. Test setup for columns

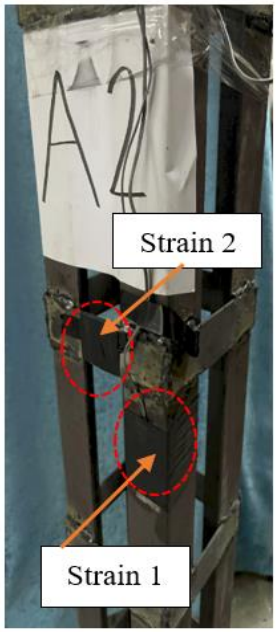

Figure 5. Location of strain gauges

3.4. Experimental Results

The experimental results are shown in **Table 5**. maximum axial load, axial displacement, horizontal displacement, ultimate axial strain, and ultimate lateral strain are among the measurement results.

Table 5. Test results

Columns	Maximum axial load P_{max} (KN)	Axial displacement at P_{max} (mm)	Horizontal displacement at P_{max} (mm)	Ultimate axial strain εs (με)	Ultimate lateral strain (με)
A1 (L50-T3-S200)	1436.9	0.768	0.502	1150	470
A2 (L50-T4-S200)	1671.9	0.682	0.423	1104	410
A3 (L50-T5-S200)	1773.3	0.618	0.401	1039	368

3.4.1. Failure Modes

There are two primary phases to the failure process. As seen in **Figure 6**, the first stage is the concrete cover crushing or spalling, and the second stage is the longitudinal reinforcement buckling. The location and value of the steel angle buckling vary depending on the thickness of the steel angles; the thicker the steel angles, the less valuable the buckling is, and the buckling is located closer to the column's middle span, such as A3 (L50-T5-200). However, the buckling of the steel angles increases with decreasing thickness and the buckling is located closer to the upper part of the column, as in the case of A1 (L50-T3-S200).

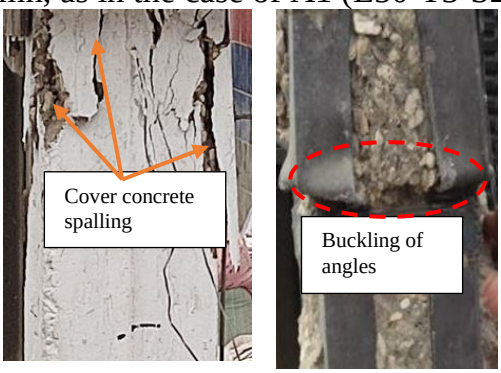

A1(L50-T3-S200)

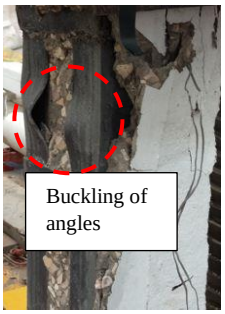

A2(L50-T4-S200) **A3(L50-T5-S200)**

Figure 6. Failure modes for tested columns.

3.4.2. Load Capacity

One of the most significant variables influencing the mechanical characteristics of the composite columns is the thickness of the steel angles. According to **Table 5** and **Figure 7;** The load capacity increases with increasing steel angle thickness. The load capacity of A2 (L50-T4-S200) and A3 (L50-T5-S200) is increased by 16% and 23%, respectively, in comparison to A1 (L50-T3-S200).

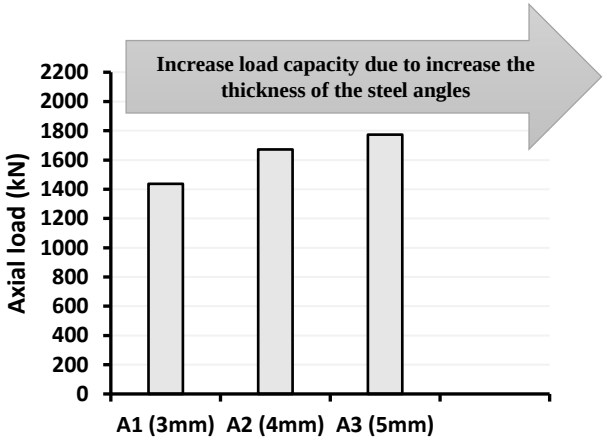

Figure 7. The effect of thickness of steel angles on load capacity

3.4.3. Effect of Steel Angles Thickness on Behavior of Composite Columns

The effect of steel angle thickness on axial displacement, horizontal displacement, axial strain, and lateral strain was depicted in **Figures 8, 9, 10, and 11.** In comparison to A1 (L50-T3-S200); A2(L50-T4-S200) and A3(L50-T5-S200) have axial displacement reductions of 11% and 20%, respectively, and horizontal displacement reductions of 16% and 20%, respectively. Furthermore, the lateral strain decreased by 13% for A2(L50-T4-S200) and 22% for A3(L50-T5-S200), while the axial strain is decreased by 4% for A2(L50-T4-S200) and 10% for A3(L50-T5-S200).

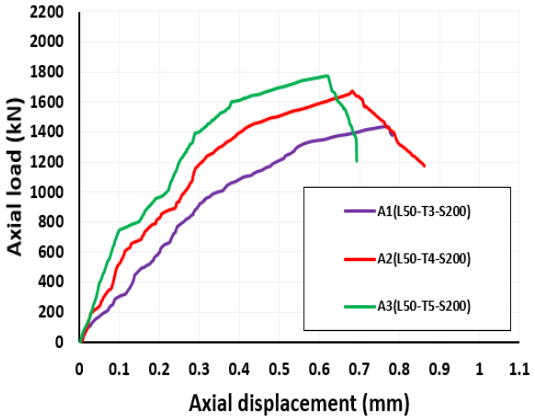

Figures 8. The effect of thickness of steel angles on axial displacement

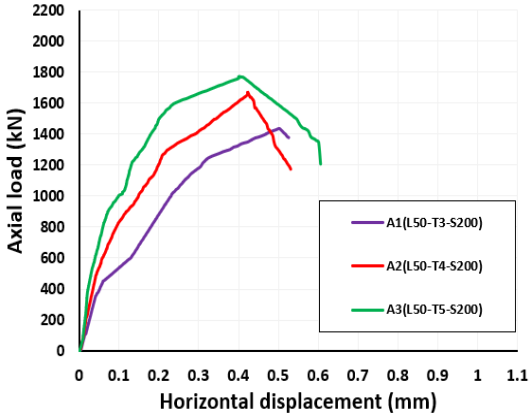

Figures 9. The effect of thickness of steel angles on horizontal displacement

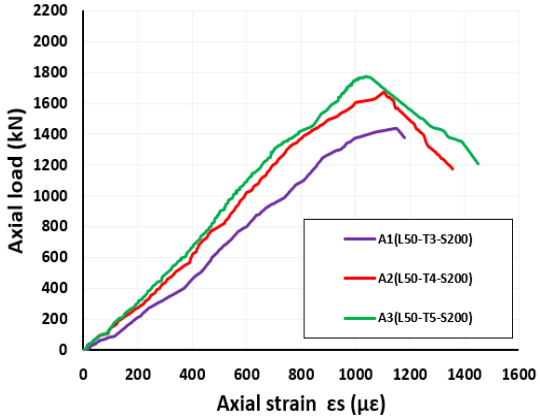

Figures 10. The effect of thickness of steel angles on axial strain

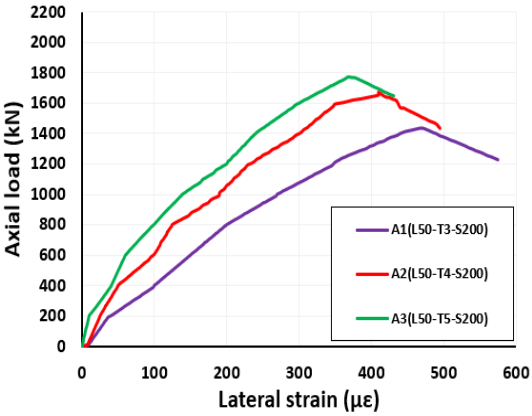

Figures 11. The effect of thickness of steel angles on lateral strain

4. Analytical Works:

The analytical studies were created using the ANSYS 19 software's finite element model (FEM). These analytical works were carried out to ensure that they were consistent with the experimental results. Then, further analytical works were created to aid in the investigation of the effects of numerous parameters.

4.1. Element types

The element types for finite element model are shown in Table 6. The **SOLID 65** element was used to model concrete. This element is used for 3-D modeling of solids with or without reinforcing bars (rebar). The solid is capable of cracking in tension and crushing in compression. A **SHELL181** element was used to model steel angles and transverse plates. This element is suitable for analyzing thin to moderately thick shell structures. It is a four-node element with six degrees of freedom at each node: translations in the x, y, and z directions, and rotations about the x, y, and z-axes. **SOLID185** is used for 3-D modeling of solid structures. It is defined by eight nodes having three degrees of freedom at each node: translations in the nodal x, y, and z directions. The element has plasticity, hyper elasticity, stress stiffening, creep, large deflection, and large strain capabilities.

4.2. Real Constants and sections

Real constant Set 1 with volume ratio equal zero is used for the solid 65 element to model plane concrete. The steel angles are defined by sections with thickness 3, 4 and 5 mm.

4.3. Material Properties

For **SOLID 65** element, the linear isotropic and multi-linear isotropic material properties are defined to model concrete. The linear isotropic properties are defined by the modulus of elasticity Ex was based on equation $\mathbf{E_x = 4400\sqrt{f'_c}}$, which f'_c is specified compressive strength of concrete and the passion's ratio. The multi-linear curve is used to help with convergence of the nonlinear solution algorithm. **Figure 12** shows the stress strain curve used in this study. The compressive uniaxial stress-strain relationship for the concrete model was divided into two parts. The first part shows the linear elastic zone up to point 1 with stress equal 0.3 f'_c. The second part from point 2 to 6 shows the elastic-plastic zone at the maximum compressive stress of concrete material, which obtained from stress $\mathbf{f = \frac{E_c\,\varepsilon}{1+(\frac{\varepsilon}{\varepsilon_0})^2}}$ where the strain at ultimate compressive strength $\boldsymbol{\varepsilon_0 = \frac{2\,f'_c}{E_c}}$. The point 7 is defined at $\mathbf{f'_c}$ and $\boldsymbol{\varepsilon_0}$.

The **SHELL181** element is being used for all steel reinforcement (angles and transverse plates) and it is assumed to be bilinear isotropic. The material properties for **SOLID185** which are being used for steel plates for supports and loading plate is assumed to be linear isotropic. The Material Models for **SOLID65**, **SHELL181** and **SOLID185** are shown from **Table 6 to Table 8**.

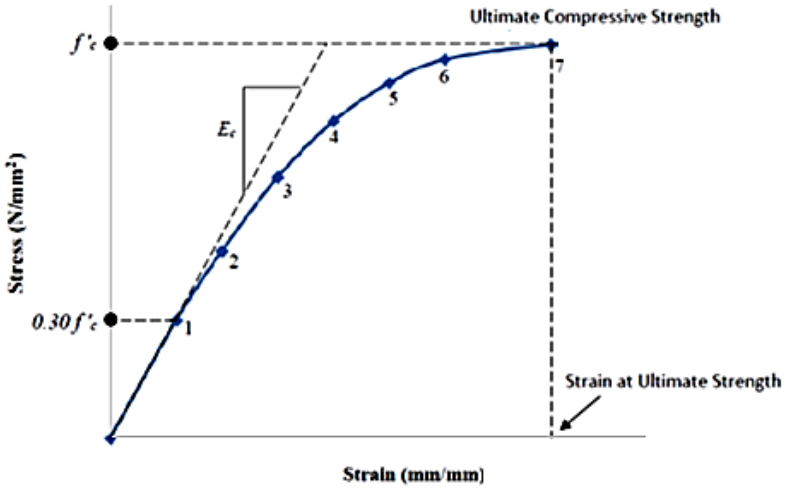

Figure 12. Uniaxial stress-strain curve for concrete

Table 6. Material models SOLID 65 for concrete

Linear isotropic		
Modulus of elasticity Ex	26872	N/mm2
Passion ratio PR xy	0.2	
Multi-linear isotropic		
Strain	Stress	N/mm2
0.00041641	11.19	
0.00061641	15.78617	
0.00081641	20.19256	
0.00101641	24.08483	
0.00121641	27.42281	
0.00141641	30.2005	
0.00161641	32.43905	
0.00181641	34.1788	
0.00201641	35.47154	
0.00221641	36.37415	
0.00241641	36.94379	
0.00277608	37.3	
0.003	37.3	
Concrete		
Open shear transfer	0.3	
Open shear transfer	0.9	
Uniaxial cracking stress	3.664	N/mm2
Uniaxial crushing stress	-1	

Table 7. Material models SHELL181 for steel angles and transverse plates

Linear isotropic		
Modulus of elasticity Ex	**200000**	**N/mm2**
Passion ratio PRxy	**0.3**	
Multi-linear isotropic		
Strain	**Stress N/mm2**	
0.001495	**326.4**	
0.41923	**417.6**	

Table 8. Material models SOLID185 for steel plates

Linear isotropic		
Modulus of elasticity Ex	**200000**	**N/mm2**
Passion ratio PRxy	**0.3**	

4.4. Modeling and Meshing

The column, plates, and supports were modeled as volumes. The model is 1200 mm total height and a cross section of (200 x 200 mm). The loading plates and steel supports are 200x200x30 mm. The steel angles were modeled as areas with leg length 50 mm and transverse plates with width 40 mm. **Figure 13 (a)** shows the Volumes and areas created in ANSYS.

To obtain good results from the Solid65 element, the use of a rectangular mesh is recommended. The volume mapped sweep command was used to mesh the steel plate, concrete and steel angles as shown in **Figure 13 (b)**. The selection of the mesh density in finite element modeling is important. A convergence of results is obtained when an adequate number of elements is used in a model, and this can be achieved when an increase in the mesh density has a negligible effect on the results. So, it was reached that the use of element mesh size equal to 30 mm is suitable that it does not consume the time in the analyses and gives accurate results.

4.5. Boundary conditions and loading

To ensure that the model acts the same way as the experimental work, boundary conditions need to be applied where the supports and loading exist in **Figure 14**. All nodes for the loading plate were given constraint in the UX, and UZ directions and all nodes under the bottom plate were given constraint in the UX, UY, and UZ directions for hinged support. The force, P, applied at each node on the steel loading plates.

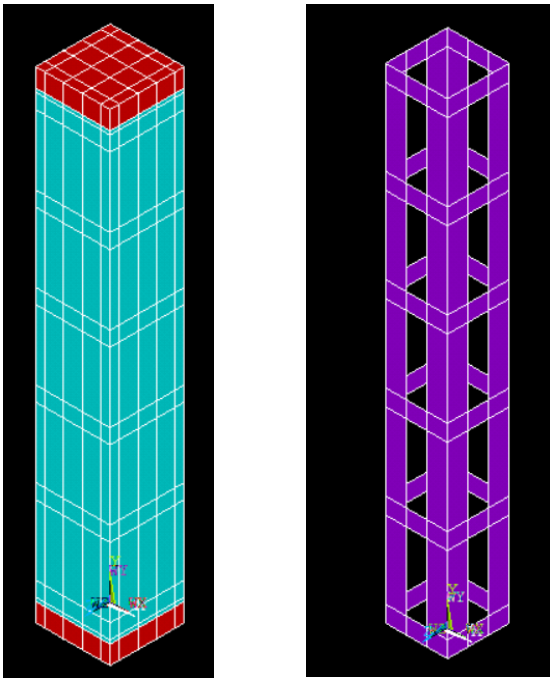

(a) (b)

Figure 13. Modeling created in ANSYS (a) Volumes for column and loading plates and (b) Angles and transverse plates.

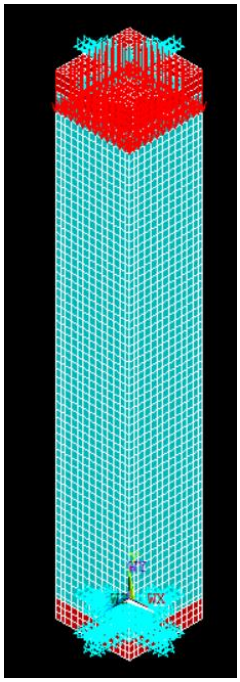

Figure 14. Meshing and boundary conditions for supports and loading plates.

4.6. Analysis Type

The static analysis type is utilized. The restart command is utilized to restart an analysis after the initial run or load step has been completed. The time at the end of the load step refers to the ending load per load step. The time step size is set to indicate load increments used for this analysis. Typical commands utilized in a nonlinear static analysis are shown in **Table 9**. All values for the nonlinear algorithm are set to defaults. The nonlinear equations are adopted using the Full Newton-Raphson method with a sufficiently large number of solution sub-steps during the loading process to capture all different stages of the behavior, including cracking, yielding, and failure. The automatic time stepping, which regulates the sub-step size according to the convergence of the solution, is as program chosen to help reduce computational time. A convergence tolerance of 5% is assumed based on the displacement degree of freedom for concrete problems.

Table 9. Commands Used to Control Nonlinear Analysis

Analysis option	Small displacement static
Calculated prestress effects	No
Time at end of load step	2000000
Automatic time stepping	On
Time step size	5000
Minimum time step	100
Maximum time step	10000
Frequency	Write every sub step

4.7. Validation for analytical model

In this section a comparison between experimental and numerical analysis for current experimental works will be illustrated in **Table 10. Figure 15** showed the load-Axial Deformation relationships for Columns A1, A2 and A3 experimentally and analytically.

As shown, the difference in load capacity between the analytical and the experimental ranged by 2 – 6 % at failure, while the difference in axial deformation is about 5-14 %. Therefore, the analytical model can be used to validate experimental work and can be used for further parametric studies.

Figure 16 shows the comparison between the failure modes experimentally vs. concrete and steel reinforcement stresses analytically for Columns A1, A2 and A3. As shown the failure location in the FE models indicated by the max values of Von Mises stresses coincided with what occurred in the experimental ones.

Table 10. Comparison between experimental and numerical analysis

Columns	Pmax (kN)			Max Axial displacement (mm)		
	Experimental	Analytical	%	Experimental	Analytical	%
A1 (L50-T3-S200)	1436.9	1517.5	106%	0.768	0.701364444	91%
A2 (L50-T4-S200)	1671.9	1710.5	102%	0.682	0.646181481	95%
A3 (L50-T5-S200)	1773.3	1722.6	97%	0.618	0.530490323	86%

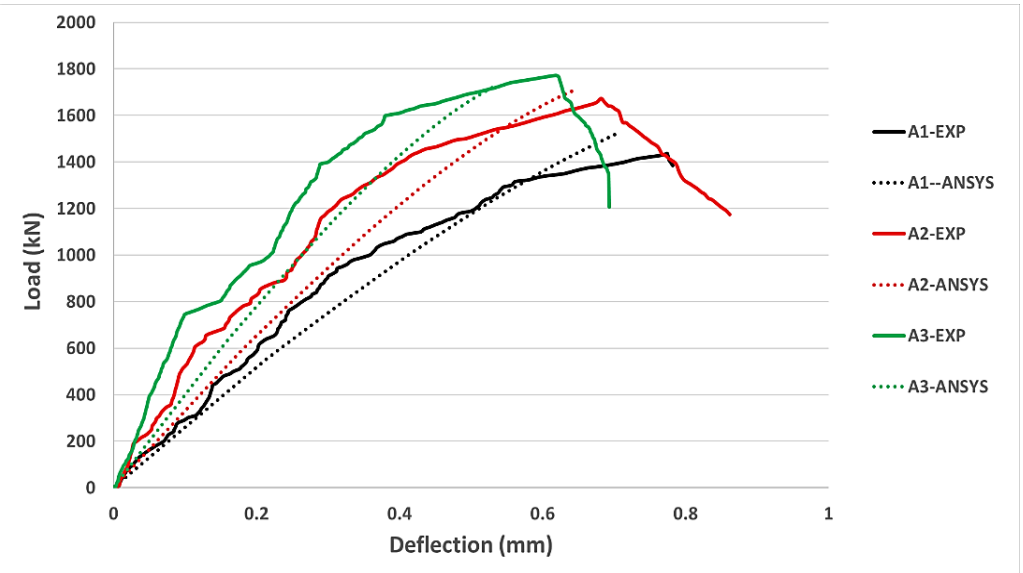

Figure 15. Load-axial deformation relationships for columns A1, A2 and A3 experimentally and analytically

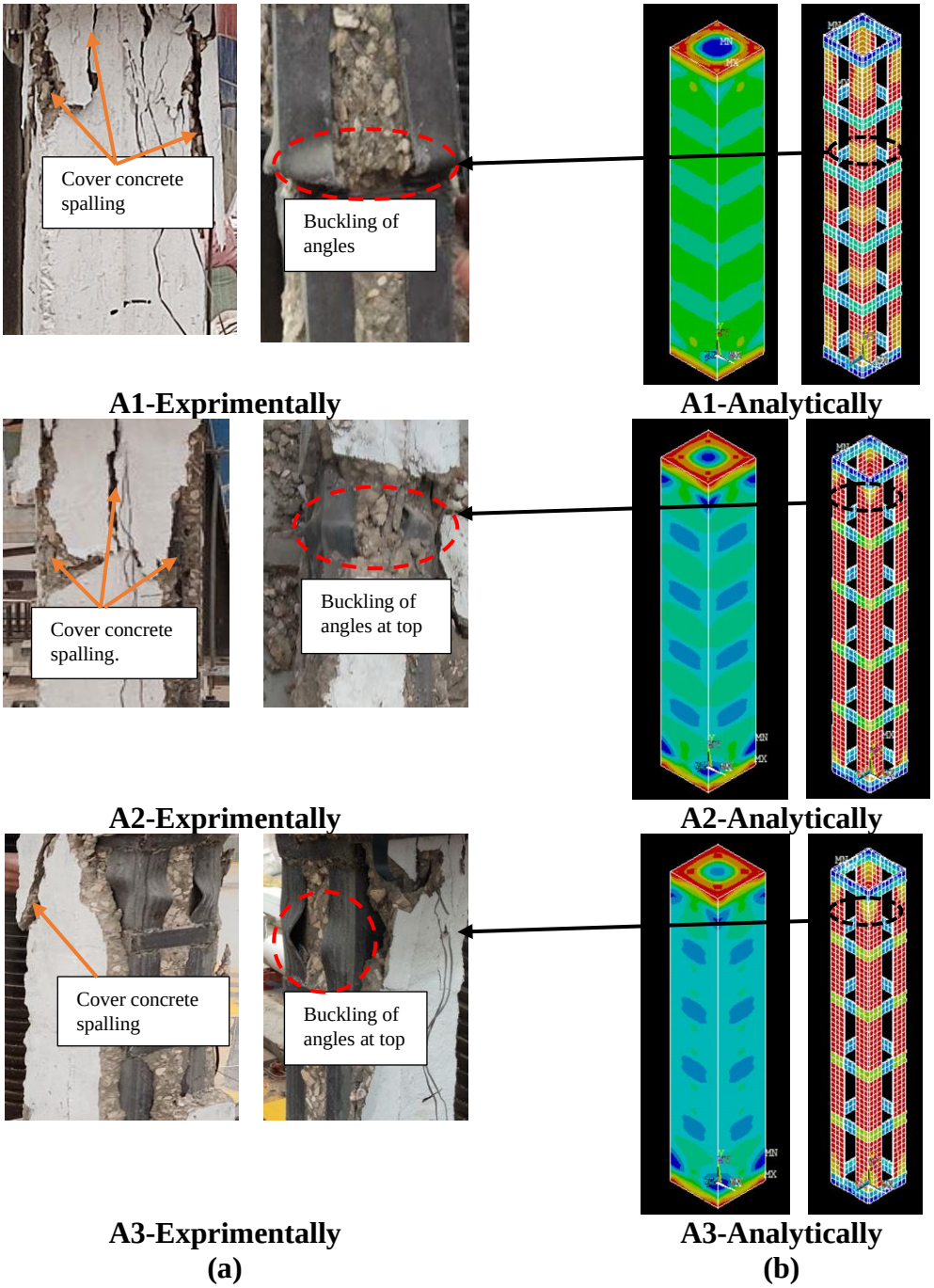

Figure 16. Failure modes experimentally vs. concrete and steel reinforcement Von Mises stresses analytically for Columns A1, A2 and A3

5. Parametric Works:

This part of the study is focused on the effect of slenderness ratio on the load capacity and axial deformation for columns A1, A2 and A3 as shown **Table 11**. Nine models were conducted to examine the impact of varying column heights: which taken 1200 mm, 1800 mm, and 2400 mm with slenderness ratios equal 6, 9, and 12 as short, medium, and slender columns. The energy absorption for each column are calculated as area under load- deformation curve.

5.1 Effect of slenderness ratio

The larger the height of the column, the lower the load capacity, the percentage of decrease in the axial load reduction varies from 4% to 6 % for samples A1, from 2% to 4 % for samples A2, and finally approaches 1 % for samples A3 with increasing the slenderness ratio from 6 to 12, as indicated by **Table 11 and Figure 17.** The closeness of the loads to each other for the same sample, despite the difference in the column height, can be explained by the absence of a noticeable buckling in the samples. Also conclude from this that as the height of the column increase and the thickness of the steel angle increase, the effect of the column height decreases as long as no noticeable buckling occurs.

The effect of increasing column height is evident in **Table 11 and Figure 17**, where a larger axial displacement is associated with higher column heights. For samples A1, A2, and A3, the percentage increase in axial displacement varies from 33 to 71%, 30 to 62%, and 30 to 58%, respectively with increasing the slenderness ratio from 6 to 12.

The energy absorption is increased with increasing the slenderness ratio for thinner reinforced angle, while the energy absorption is decreased with increasing the slenderness ratio for thicker reinforced angle.

It can be noticed that higher the slenderness ratio where having the same reinforced angle thickness led to more the axial deformation with neglectable effect on load capacity. This notice in evident for columns with thinner reinforced angle than thick reinforced angle.

5.2 Effect of reinforcing steel angles thickness

The effect of reinforced angle thickness with varying the slenderness ratio of columns is conducted. For columns A1, A2, and A3 with slenderness ratio equal 6; as short columns, increasing the angle thickness (from 3 mm to 5 mm) led to increase the load capacity with 13% to 14% and decrease the axial deformation with 8% to 18%. As medium columns, columns A1, A2, and A3 with slenderness ratios of 9 showed an improvement in load capacity of 15% to 17% and a decrease in axial deformation of 10% to 18% with an increase in angle thickness of 3 mm to 5 mm. In the case of columns A1, A2, and A3, which have a slenderness ratio of 12, raising the angle thickness (from 3 mm to 5 mm) resulted in a 15% to 19% improvement in load capacity and an 18% to 20% decrease in axial distortion.

It can be noted that increasing the thickness of the reinforcing steel angle for slender columns has more improvement in load capacity than short columns; on the other hand; this led to more reduction in axial distortion.

Table 11. Load – deflection results for columns based on parametric study

Samples	Column height (mm)	Slenderness ratio (λ)	Max. failure load (kN)			Max. Axial deformation (mm)			Energy absorption (Joule)		
			P_{max}	Ratio w.r.t	Ratio w.r.t	Δ_{max}	Ratio w.r.t	Ratio w.r.t	J	Ratio w.r.t	Ratio w.r.t
A1 (L50-T3-S200)	1200	6	1517.5	-	-	0.7014	-		317.4	-	-
	1800	9	1457.5	0.96	-	0.9318	1.33		495.7	1.56	-
	2400	12	1427.5	0.94	-	1.1994	1.71		809.5	1.63	-
A2 (L50-T4-S200)	1200	6	1710.5	-	1.13	0.6462	-	0.92	342.5	-	1.08
	1800	9	1676.7	0.98	1.15	0.8394	1.3	0.9	522.4	1.53	1.05
	2400	12	1647.3	0.96	1.15	1.0487	1.62	0.87	813.8	1.56	1.01
A3 (L50-T5-S200)	1200	6	1722.6	-	1.14	0.5305	-	0.76	230.3	-	0.73
	1800	9	1710.3	0.99	1.17	0.6905	1.3	0.74	387.1	1.68	0.78
	2400	12	1698.6	0.99	1.19	0.8399	1.58	0.7	554.5	1.43	0.68

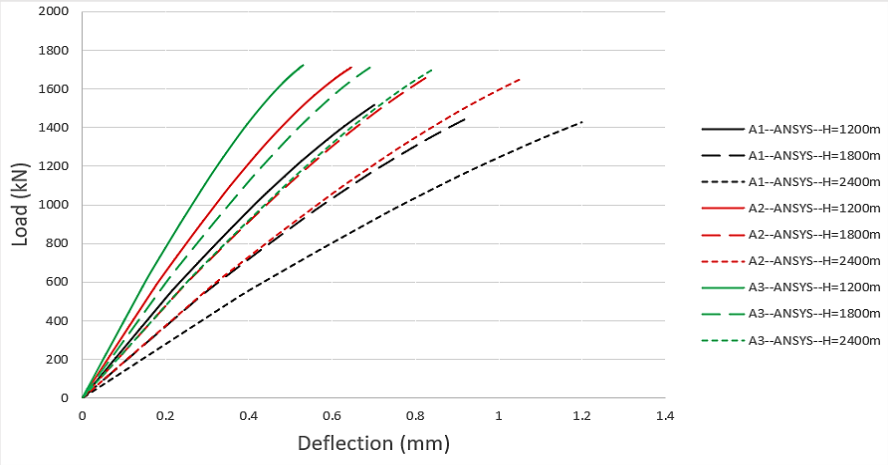

Figure 17. The effect of slenderness ratio on load-axial deformation relationships for columns A1, A2 and A3 analytically

6. Conclusions:

The mechanical characteristics of composite concrete columns with welded batten transverse reinforcement and steel angle longitudinal reinforcement were examined. The following is a summary of the most important results obtained:

1. There are two primary phases to the failure process. Localized buckling in the

longitudinal reinforcement occurs in the second stage, after the concrete cover has been crushed or spalled in the first stage.

2. The impact of steel angle thickness according to experimental results: axial strain, lateral strain, horizontal displacement, and axial displacement decrease with increasing steel angle thickness. The percentage of decrease for axial displacement is between 11% and 20%; for horizontal displacement, it is between 16% and 20%; for axial strain, it is between 4% and 10%; and for lateral strain, it is between 13% and 22%. But the load capacity increases with increasing steel angle thickness, the percentage of increase for load capacity is between 16% and 23%.
3. The convergence rate between the finite element model and the experimental results ranged from 2% to 6% for load capacity and ranged from 5% to 14% for axial displacement. This means that an analytical model using ANSYS software was presented a reliable prediction of the failure load and axial deformation and can capture the failure modes.
4. Higher the slenderness ratio where having the same reinforced angle thickness led to more the axial deformation with neglectable effect on load capacity. This notice in evident for columns with thinner reinforced angle than thick reinforced angle.
5. As the height of the column increase and the thickness of the steel angle increase, the effect of the column height decreases if no noticeable buckling occurs.
6. Increasing the thickness of the reinforcing steel angle for slender columns has more improvement in load capacity than short columns; on the other hand; this led to more reduction in axial distortion.
7. For thinner reinforced angles, the energy absorption increases as the slenderness ratio increases, but for thicker reinforced angles, the energy absorption decreases as the slenderness ratio increases.

7. Recommendation

It is advised to investigate a few factors that were not considered in this study: (a) the impact of steel angle openings; (b) the effect of changing the width of the battens. One should consider sanding or covering the steel angles in a steel net to improve the cohesiveness between the steel angles and the concrete cover.

8. References

M. H. KIM, H. G. KIM, Y. K. Ju and S. D. KIM "Experimental Study on the Axial Behavior of yLRC Composite Columns" Procedia Engineering 14 (2011) 2058–2063, doi:10.1016/j.proeng.2011.07.258.

Piotr Lacki, Anna Derlatka and Przemysław Kasza "Comparison of steel-concrete composite column and steel column" Composite Structures 20 November 2017, doi.org/10.1016/j.compstruct.2017.11.055.

T. Hemanth Kumar and K. Shankar Sai "EXPERIMENTAL STUDY ON AXIALLY LOADED COMPOSITE COLUMNS" 653INTERNATIONAL JOURNAL OF INFORMATION AND COMPUTING SCIENCE, Volume 6, Issue 6, June 2019.
Youyou Zhang, Yuqing Liu, Haohui Xin, Jun He "Numerical parametric study on ultimate load and ductility of concrete encased equal-leg angle steel composite columns" Engineering Structures 200 (2019) 109679.
Hyeon-Jin Kim, Hyeon-Jong Hwang, Hong-Gun Park "Flexural testing for composite members with bolt-connected steel angles" Engineering Structures 230 (2021) 111638 doi.org/10.1016/j.engstruct.2020.111638.
Hyeon-Jin Kim, Hyeon-Jong Hwang, Hong-Gun Park, Dong-Kwan Kim "Concentric axial load test for composite columns using bolt-connected steel angles" Engineering Structures 214 (2020) 110650.
V. Badalamenti, Campione, and M. L. Mangiavillano "Simplified Model for Compressive Behavior of Concrete Columns Strengthened by Steel Angles and Strips" JOURNAL OF ENGINEERING MECHANICS © ASCE / FEBRUARY 2010,
DOI: 10.1061/_ASCE_EM.1943-7889.0000069.
Tae-Sung Eom, Jong-Jin Lim and Jin-Won Kim "Axial Compressive Behavior of Concrete-Encased High-Strength Steel Angle Columns" © 2021 American Society of Civil Engineers, DOI: 10.1061/ (ASCE) ST.1943-541X.0002908.
(Chang-Soo Kim, Ph.D), (Hong-Gun Park, M.ASCE), (Kyung-Soo Chung, Ph.D.) and (In-Rak Choi, Ph.D) " Eccentric Axial Load Capacity of High-Strength Steel-Concrete Composite Columns of Various Sectional Shapes" © 2013 American Society of Civil Engineers.
(Tae-Sung Eom), (Hyeon-Jong Hwang), (Hong-Gun Park, M. ASCE), (Chang-Nam Lee) and (Hyoung-Seop Kim) "Flexural Test for Steel-Concrete Composite Members Using Prefabricated Steel Angles" © 2013 American Society of Civil Engineers.
Ranga Rao Vummaneni and M. Achyutha Kumar Reddy "Performance of composite reinforced short column under axial loading" Article *in* International Journal of Engineering & Technology · July 2018.
Hyeon-Jong Hwang "Prefabricated Steel-Reinforced Concrete Composite Column" © 2018 the Author(s). Licensee IntechOpen.
Chang-Soo Kim, and Hyeon-Jong Hwang "Numerical Investigation on Load-carrying Capacity of High-strength Concrete-encased Steel Angle Columns" International Journal of Concrete Structures and Materials (Received January 14, 2017, Accepted January 7, 2018).
Ayoob A. Ibrahim, M. Neaz Sheikh, Muhammad N. S. Hadi "Axial Compressive Behavior of Steel Equal Angle Section- Reinforced Square High-Strength Concrete Column" Faculty of Engineering and Information Sciences - Papers: Part B. 2712 (2018).
Chong Rong, Qingxuan Shi "Behaviour of angle steel frame confined concrete columns under axial Compression" Construction and Building Materials 241 (2020) 118034.